Korean J Physiol Pharmacol
Vol 15: 371−382, December, 2011
http://dx.doi.org/10.4196/kjpp.2011.15.6.371

A Computational Model of the Temperature-dependent Changes in Firing Patterns in *Aplysia* Neurons

Nam Gyu Hyun[1,*], Kwang-Ho Hyun[2], Kwang-Beom Hyun[2], Jin-Hee Han[3], Kyungmin Lee[4], and Bong-Kiun Kaang[5,†]

[1]Department of Physics, Jeju National University, Jeju 690-756, [2]Department of Biological Sciences, Korea Advanced Institute of Science and Technology, [3]Department of Biological Sciences, KAIST Institute for the Bio Century (KIB), KAIST, Daejeon 305-701, [4]Department of Anatomy, Graduate School of Medicine, Kyungpook National University, Daegu 700-422, [5]National Creative Research Initiative Center for Memory, Departments of Biological Sciences and Brain and Cognitive Sciences, College of Natural Science, Seoul National University, Seoul 151-747, Korea

We performed experiments using *Aplysia* neurons to identify the mechanism underlying the changes in the firing patterns in response to temperature changes. When the temperature was gradually increased from 11°C to 31°C the firing patterns changed sequentially from the silent state to beating, doublets, beating-chaos, bursting-chaos, square-wave bursting, and bursting-oscillation patterns. When the temperature was decreased over the same temperature range, these sequential changes in the firing patterns reappeared in reverse order. To simulate this entire range of spiking patterns we modified nonlinear differential equations that Chay and Lee made using temperature-dependent scaling factors. To refine the equations, we also analyzed the spike pattern changes in the presence of potassium channel blockers. Based on the solutions of these equations and potassium channel blocker experiments, we found that, as temperature increases, the maximum value of the potassium channel relaxation time constant, $\tau_n(t)$ increases, but the maximum value of the probabilities of openings for activation of the potassium channels, n(t) decreases. Accordingly, the voltage-dependent potassium current is likely to play a leading role in the temperature-dependent changes in the firing patterns in *Aplysia* neurons.

Key Words: *Aplysia*, Bursting, Doublet, Temperature-dependent scaling factor, Computer simulation

INTRODUCTION

It is well known that the general conclusion from other studies on the temperature dependence of firing patterns of *Aplysia* neurons was the increase in spike frequency [1,2], an increase in resting membrane potential [1,3], and a decrease in spike-broadening and spike height [4] with increasing temperature. For example, Hakozaki et al. found that temperature-induced hyperpolarization was mediated in *Aplysia* neurons by the temperature-sensitive and G-protein regulated potassium current as the temperature increased [5]. AP broadening in *Aplysia* R15 pacemaker neuron resulted from the depolarizing effect of slow voltage-dependent Ca^{2+} currents and its peak height was decreased by steady activation of a temperature-sensitive K^+ current [4]. However, the mechanisms of the firing pattern changes in response to temperature are still unclear. To identify the mechanism of the temperature-induced firing pattern change, we examined the effect of temperature on the firing pattern by using the neurons of *Aplysia* and developed a computational model to simulate the temperature-dependent changes in the firing patterns.

Aplysia neurons have great advantages for electrophysiological study. In *Aplysia*, the nervous system is relatively simple and the size of individual neuron is so large that each neuron can be easily identified based on the location in the ganglia. In addition, *Aplysia* giant neurons are long-lived in vitro and so are apt to stand heat stress for a long time. The neurons in the left caudal quarter-ganglion (LUQ) of the abdominal ganglion of *Aplysia* fires spontaneously. We found that many of these neurons in the LUQ changed the firing pattern sequentially with temperature from a silent state to beating, beating-chaos, bursting-chaos, square-wave bursting, and finally a burst-

Received October 5, 2011, Revised November 1, 2011, Accepted November 2, 2011

*Corresponding to: Nam Gyu Hyun, Department of Physics, Jeju National University, 1, Ara-dong, Jeju 690-756, Korea. (Tel) 82-64-754-3513, (Fax) 82-64-756-3506, (E-mail) nhyun@jejunu.ac.kr
†Co-corresponding to: Bong-Kiun Kaang, Department of Biological Sciences, Seoul National University, 599, Gwanangno, Gwanak-gu, Seoul 151-747, Korea. (Tel) 82-2-880-7525, (Fax) 82-2-884-9577, (E-mail) kaang@snu.ac.kr

ABBREVIATIONS: TEA, tetraethylammonium chloride; 4-AP, 4-Aminopyridine; AP, action potential; ISI, the interspike interval; IBI, the interburst interval; ASW, artificial seawater; DAQ, data acquisition; ID, interval duration.

ing-oscillation pattern. When the temperature was decreased over the same temperature range, the above seven patterns reappeared in reverse order.

Based on these experimental results, we wanted to compose equations to simulate all of the seven different spiking patterns. However, we found that these various signal patterns observed between 25°C and 31°C were similar to pictures published by Chay [6], and Chay and Lee [7]. Although in these papers various spiking patterns were described by solving nonlinear differential equations such as continuous spiking, doublets, beating-chaos, bursting-chaos, square-wave bursting, and slow-wave, the silent phase and low frequency beating were not described between 11°C and 25°C that are observed in our experiments. Furthermore, any temperature-dependent scaling factors were not included in these equations, either. Therefore, simply changing the variables presented in papers by Chay and Lee [6,7] would not be sufficient to simulate these exceptional spiking patterns. Furthermore it was uncertain whether or not the temperature-dependent neurons from the abdominal ganglion of *A. juliana* could be regarded as warm receptors. Because cold and warm receptors respond to temperature change in one direction only; warm (cold) receptor responds to temperature changes during the rising (falling) phase but do not respond to temperature changes during the falling (rising) phase. Therefore, these neurons are thought to be different from warm receptors. However, the effects of temperature changes on cold or warm receptors have been studied in various species, including cats [8,9], vampire bats and mice [10], snakes [11], rabbit [12], and human [13]. Although mammalian cold receptors are discussed in the Huber-Braun cold receptor model [14,15], it was not even able to find a proper biophysical model for warm receptors.

To set up nonlinear differential equations that can simulate all of these various spiking patterns together, it is necessary to modify the equations derived by Chay and Lee [6,7] with temperature-dependent scaling factors; we will adopt a temperature-dependent scaling factor for the ionic currents and ionic kinetics that are used in the Huber-Braun cold receptor model [14,15]. The cell membrane of this new model contains sodium, calcium, and potassium channels carrying a fast sodium current, I_{Na}, fast calcium current, I_{Ca}, and a potassium current, I_K, respectively. But when channel blockers are used, we can find out how the spiking patterns change. After we focus on finding out the relationships between channel blockers and AP change, we will examine the mechanism of electrophysiological response to temperature change in neural cells in *Aplysia*.

METHODS

Animals and preparation of the ganglia

Aplysia juliana and *Aplysia kurodai* were purchased by a local supplier in Jeju-do, South Korea. The species are identified according to the literature [16].

When an *Aplysia* was to be dissected, 0.38 M $MgCl_2$ were injected for anesthesia. $MgCl_2$, amounting to half weight of the *Aplysia*, were injected. With dissecting tools, the abdominal ganglia of *A. juliana* were dissected out and preserved in artificial seawater ASW : L-15 (1 : 1, v/v) as described previously [16]. The abdominal ganglia incubated at 34°C for about one hour in 1% protease (type IX, sigma) in ASW : L-15. The ganglia treated with protease were washed several times with ASW, and were stored at 18°C for about five hours. Finally, the ganglion was pinned down on a Sylgard plate dish (50×9 mm) and the sheaths of the ganglia were dissected out under dissecting microscope to expose the neurons on the dorsal side of the abdominal ganglion. The medim was exchanged with L-15/ASW.

Data acquisition

The Sylgard plate containing the ganglion was placed on a small copper plate (50×100 mm) under which two thermoelectric controllers were set up (HMN 3940, Acetec Co., Korea) side by side. One with the hot side was faced down and the other with the cold side was faced down. We installed an automatic temperature controller. The data acquisition (DAQ) card (NI PCI-6221, National Instruments) was connected between the Neuroprove Amplifier (Model 1600, A-M Systems, Carlsborg, WA, USA) and the computer. The membrane potential was recorded intracellularly using the Neuroprove Amplifier with a glass microelectrode filled with 3 M KCl. and was sent to channel 2 of the data acquisition device. For the measurement of the temperature near the recording neurons, the PT100 temperature probe was placed near the *Aplysia* ganglion. To record the temperature, we used a digital thermometer (TRM-006, Toho, Japan) connected to a PT100 temperature sensor through channel 1 of the DAQ card. The values of temperature and membrane potential were simultaneously saved onto the computer hard disk. We used the computer program previously coded for another experiment. Some parts were modified and reused in this experiment. In data analysis program, various variables were calculated. Most significant variables are the AP amplitude A_{AP} (mV), the membrane potential at the negative peak V_{np} (mV), the interspike interval ISI (ms), the AP half-width duration $\Delta t_{AP,\,1/2}$ (ms), the interburst interval IBI (ms), and the spontaneous firing frequency Frequency (s^{-1}) [17].

Drug application

Tetraethylammonium chloride (TEA, Sigma: T2265), 4-aminopyridine (4-AP, TCI: A0414) are purchased from Sigma-Aldrich and TCI Co. LTD. By using a pump (BT100-2J, LongerPump, Hebei, China), L-15 : ASW (1 : 1), 10 mM TEA, L-15 : ASW (1 : 1), 10 mM 4-AP, L-15 : ASW (1 : 1), 10 mM TEA mixed with 10 mM 4-AP were pumped in consecutive order at a rate of 1 ml/min for 30 minutes, respectively. This is one cycle. We knew that the concentration of chemical reagents was at maximum within about five minutes before and after each drug treatment, and cells were adapted to it. In these time intervals, cells showed steady results. So, neurosignals were analyzed using the data recorded during these periods.

RESULTS

Experimental data for analysis

To simulate temperature-dependent properties of the APs, we performed experiments using *Aplysia* neurons. In these experiments, the cells showed a bursting-oscillation pattern at temperatures between 28.8°C and 32.2°C and then became silent when the temperature was increased

Table 1. Dissection and electrophysiological properties for the experiments A to E and details of the seven different firing patterns observed in the acquired data. Silent, beating (bursting with very long burst duration and short interburst intervals), doublet, beating chaos, bursting chaos, bursting, and bursting oscillation patterns are shown

Dissection, electrophysiol. properties and patterns of temperature dependence of APs		Experimental data				
		Experiment A	Experiment B	Experiment C	Experiment D	Experiment E
Species of animals (weights of animals (g))		*A. juliana* (220)	*A. juliana* (97)	*A. juliana* (358)	*A. kurodai* (316)	*A. juliana* (420)
Seasons of experiments		spring	summer	spring	spring	spring
Size and positions of cells		Giant, d.s. of lcq	Giant, d.s. of lcq	Giant, d.s. of lcq	Giant, d.s. of lcq	Medium-s., d.s. of lcq
Media (ext. cell fluid)		L-15 : ASW (1 : 1, v/v)	L-15 : ASW (1 : 1, v/v)	L-15 : ASW (1 : 1, v/v)	L-15 : ASW (1 : 1, v/v)	L-15 : ASW (1 : 1, v/v)
Range of tem. change (°C)		10.0～31.3	11.1～32.4	13.5～30.1	12.8～30.5	6.9～26.6
Total time for recording (min)		351	1,632	360	1,079	2,719
Total number of spikes		35,983	125,487	35,671	90,344	92,257
Average firing rate (min^{-1})		102.5	76.8	99.0	83.7	33.9
Sel. dur. for anal. (min)		35	55	29	66	59
Patterns of temp. dependence of APs (°C)	Silent	10.9～11.5	11.1～14.0	13.5～13.6		9.6～10.1
	Beating	11.5～24.5	14.0～26.8	15.0～26.0	15.2～27.2	10.1～23.5
	Doublet	24.5～26.3	26.8～27.1	26.0～26.9	27.2～27.7	23.7～24.0
	Beating-chaos	26.3～27.1	27.1～28.0	26.9～27.9	27.7～27.8	24.0～24.3
	Bursting-chaos	27.1～28.4	28.0～28.7	27.9～28.4	27.8～28.0	24.3～24.9
	Square-wave bursting	28.4～30.0	28.7～30.2	28.4～28.8	28.0～28.9	24.9～25.9
	Bursting-oscillation	30.0～31.0	30.2～32.2	28.8～30.1	28.9～31.2	

Ext. cell fluid, external cell fluid; d.s. of lcq, dorsal surface of the left caudal quarter-ganglion; Sel. dur. for anal., selected section duration for analysis; Patterns of temp. dependence of APs, Patterns of temperature dependence of APs.

over about 35°C. However, the temperature had to be reduced to prevent the cell from becoming silent after the bursting-oscillation pattern appeared because the silent state at high temperature could influence the activity of APs.

Table 1 shows the conditions of each experiment (Experiment A to E). In these experiments the species *A. juliana* and *A. kurodai* were used. Only large cell somata bigger than ~100 micron were selected for recording and these neurons were located at the dorsal surface of the left caudal quarter-ganglion. The temperature was controlled between 6.9°C and 32.4°C. The total length of time for recording was between 351 and 2,719 min. The total number of spikes recorded from each neuron was from 35,983 to 125,487. The average firing rate was between 33.9 min^{-1} and 102.5 min^{-1}. The duration of recording sections subjected to data analysis varied from 29 to 66 min. In Table 1, we selected the five datasets of the experiments that showed the following seven spiking patterns sequentially as temperature increased: silent, beating (sinusoidal bursting with a very long burst duration and short interburst intervals (IBI)), doublets, beating-chaos, bursting-chaos, square-wave bursting, and bursting-oscillation. In these experiments when the temperature was decreased over a similar range, the above seven patterns reappeared in reverse order. For each of the five separate experiments the temperature intervals corresponding to each spiking pattern are presented at the bottom of Table 1, suggesting that the firing pattern is likely determined by the instantaneous temperature; there were no data acquired below 15.2°C in Experiment D (no silent state), and above 25.9°C in Experiment E (no bursting-oscillation).

Fig. 1 displays the averaged values of AP parameters as a function of temperature. The IBI has larger errors bars than the other AP parameters. The A_{AP}, $\Delta t_{AP, 1/2}$, and ISI

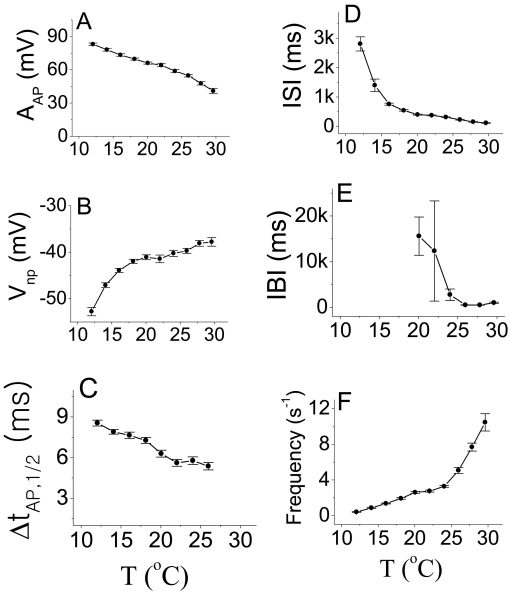

Fig. 1. Average values of six AP parameters with error bars. A_{AP}, $\Delta t_{AP, 1/2}$, ISI, and IBI displayed in panels A, C, D, and E, respectively, decreased as temperature increased. $|V_{np}|$ and Frequency displayed in panels B and F, respectively, increased as temperature increased.

decreased with increasing temperature. The IBI in Fig. 1 E also decreased with increasing temperature; however, the error bars in Fig. 1 E from 20°C to 24°C are relatively large because different values of the IBI in the sinusoidal bursting pattern appeared at different temperatures within

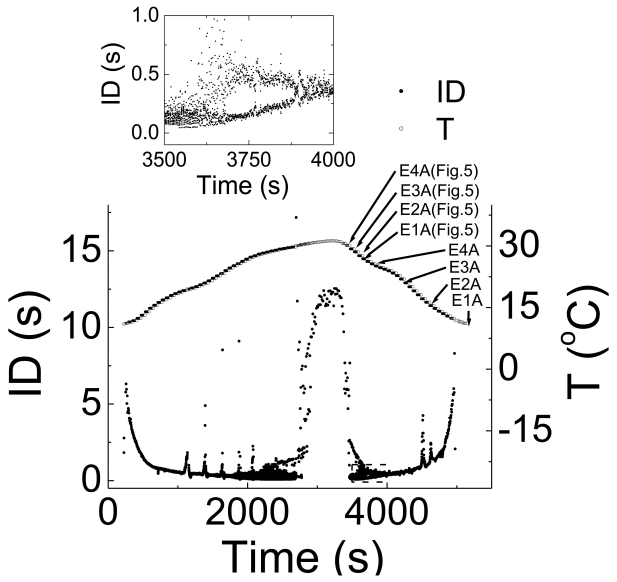

Fig. 2. Temperature and ID as a function of time. Data acquired from one temperature cycle in Experiment A are plotted. The near symmetry of the graph is taken to mean that the time-dependence of the data to be analyzed is reproducible. The small upper box displays a magnified view from 3,500 s to 4,000 s. The symbols E1A to E4A (Fig. 5), written in the large bottom box correspond to the time series displayed in each panel in Fig. 4E1A to Fig. 5E4A. Sinusoidal bursting with very long burst duration and short IBI is shown by the sign looked like "∧" in the bottom trace.

these temperature ranges. $|V_{np}|$ in Fig. 1B and the Frequency in Fig. 1 F increased with increasing temperature. Likewise, the spiking frequencies of warm (cold) receptors increase as the temperature increase (decrease).

Based on these experimental results, we wanted to compose equations to simulate all of the seven different spiking patterns. In order to do this, we selected experimental data from two of the five experiments, i.e., Experiments A and B. Although the selected data had similar firing patterns, data from Experiment A displayed more stable firing patterns, especially in the doublet, beating-chaos, bursting-chaos, and square-wave bursting patterns. For this reason we chose to use the data from Experiment A to draw multiple graphs corresponding to each spiking pattern. It was also necessary to select a section of the data containing the properties of all of the spiking patterns; for this the 80-minute data which correspond to one temperature cycle was selected from the data of Experiment A. The temperature values and interval duration (ID) of APs are presented as functions of time in Fig. 2. In this figure, it is shown that when the temperature was increased or decreased over the same temperature range, the same spiking patterns reappeared in reverse order. For example, when the temperature was decreased from 31°C to 11°C, the seven firing patterns of *Aplysia* neurons changed sequentially: bursting-oscillation, square-wave bursting, bursting-chaos, beating-chaos, doublets, beating, and silent. These spike trains in continuous time series are shown in Fig. 3. The small box at the top of Fig. 2 displays a magnified view of the IDs from 3,500 s to 4,000 s and clearly shows doublets appearing. The symbols "E1A"∼"E4A (Fig. 5)" written on the lower big plot correspond to the names of the panels

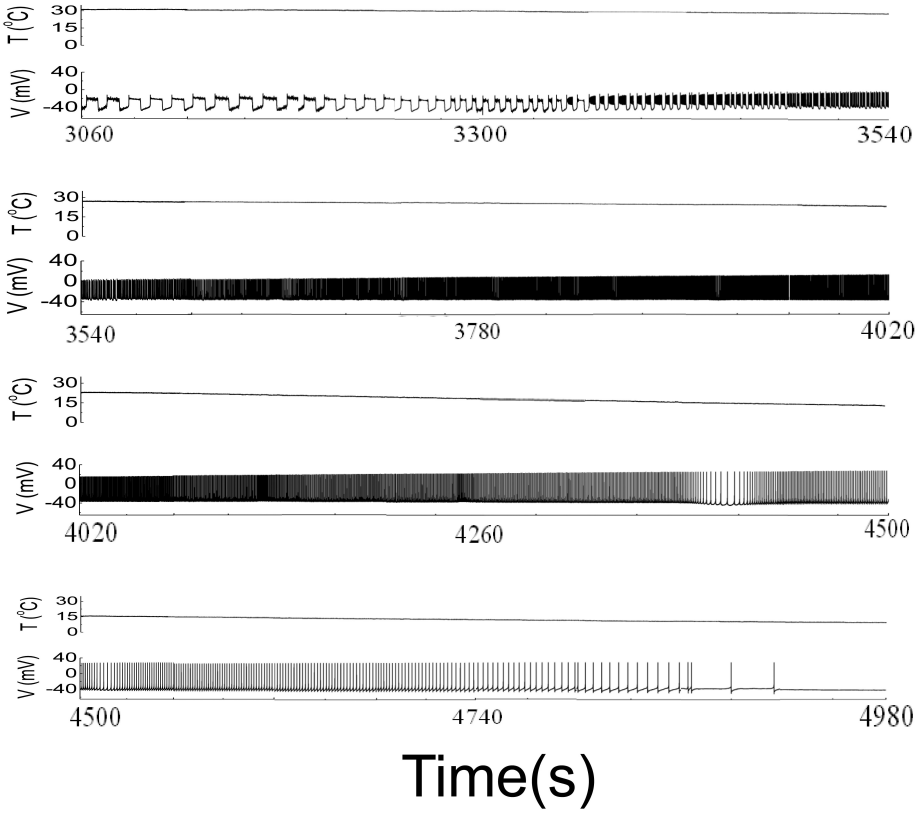

Fig. 3. The upper and lower traces represent temperature and membrane potential, respectively. When the temperature was decreased from 31°C to 11°C, the seven firing patterns of *Aplysia* neurons changed sequentially: bursting-oscillation, square-wave bursting, bursting-chaos, beating-chaos, doublets, beating, and silent.

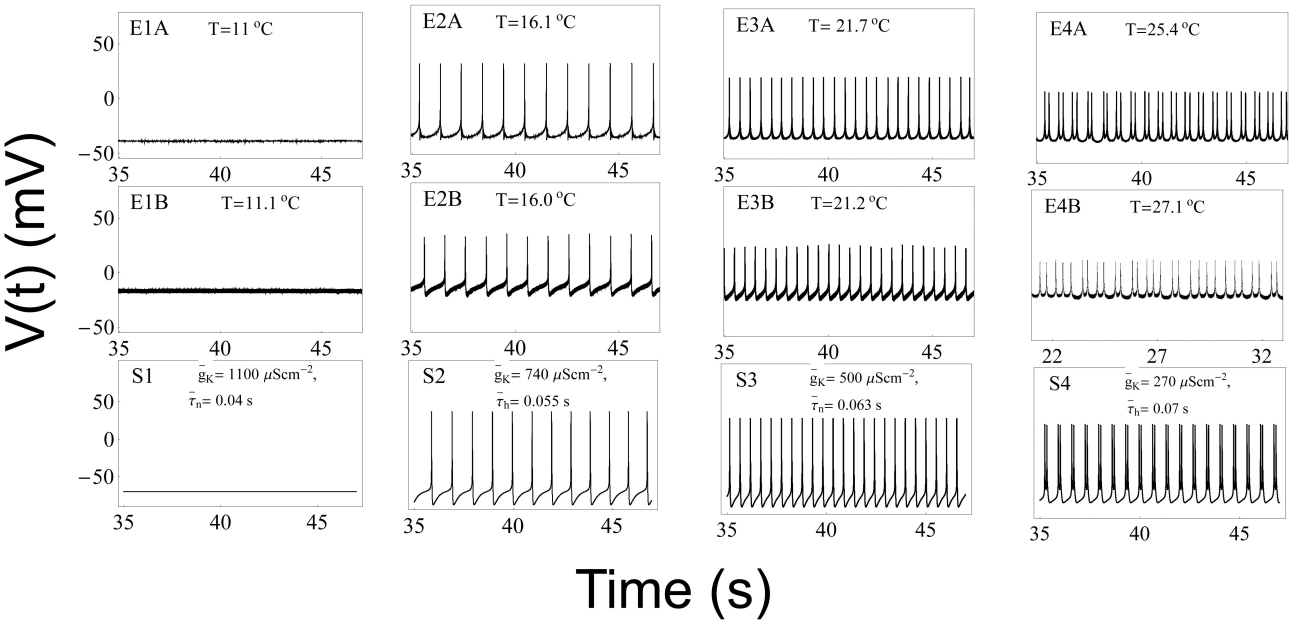

Fig. 4. Comparison of experimental results with results from computer simulations. Panels E1A～E4A display data from Experiment A. Panels E1B～E4B display data from Experiment B. The relevant temperatures are shown at the top of each box. Panels S1～S4 display values calculated from equations (1) to (4) using parameters from the type 1 model at the temperatures shown in panels E1A～E4A, respectively. The variables $\bar{g}_K$ and $\bar{\tau}_n$ used in the simulations are shown at the top of the boxes in the bottom panel of each set of three panels. Panels E1A, E1B, and S1 display silent pattern. Panels E2A, E3A, E2B, E3B, S2 and S3 display beating pattern. Panels E4A, E4B, and S4 display doublet pattern.

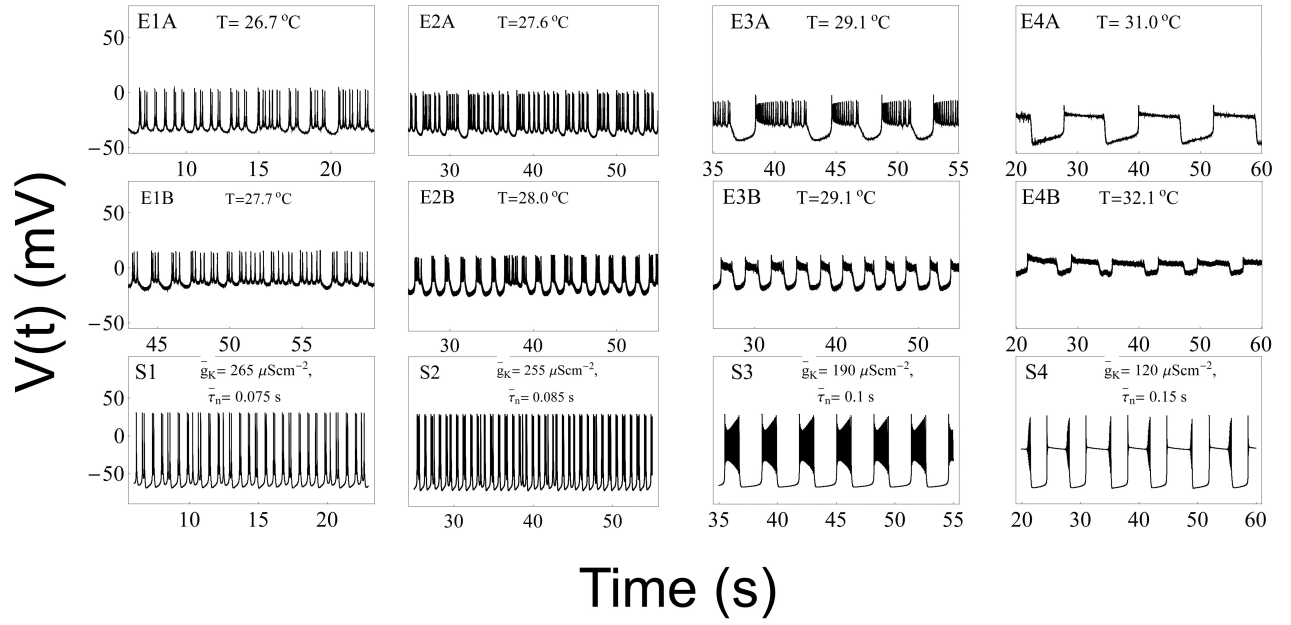

Fig. 5. Comparison of experimental results with results from computer simulations. Panels E1A～E4A display data from Experiment A. Panels E1B～E4B display data from Experiment B. The relevant temperatures are shown at the top of each box. Panels S1～S4 display values calculated from equations (1) to (4) using parameters from the type 1 model at the temperatures shown in panels E1A～E4A, respectively. The variables $\bar{g}_K$ and $\bar{\tau}_n$ used in the simulations are shown at the top of the boxes in the bottom panel of each set of three panels. Panels E1A, E1B, and S1 display beating chaos. Panels E2A, E2B, and S2 display bursting chaos. Panels E3A, E3B, and S3 display square-wave bursting. Panels E4A, E4B, and S4 display bursting-oscillation.

that are displayed in more detail in Fig. 4E1A to Fig. 5E4A, respectively. Several sinusoidal burstings with very long burst duration and short IBI are shown by the sign looked like "∧" in the bottom trace in Fig. 2. Since these signals appeared irregularly, we did not simulate these phenomena.

The model

Although the Huber-Braun cold receptor model [14,15] describes cold receptors well, proper biophysical model for warm receptors has not been searched. To set up nonlinear differential equations that could simulate all of these various spiking patterns together, it was necessary to modify the equations (Chay-Lee model) derived by Chay and Lee [6,7] with temperature-dependent scaling factors; we adapted the temperature-dependent scaling factors for the ionic currents, $\rho(T)$, and for the ionic kinetics, $\phi(T)$, that are used in the Huber-Braun cold receptor model. To consider a temperature-dependent scaling factor for reversal potentials (or Nernst potentials), a new temperature-dependent scaling factor, $\sigma(T)$, was defined and used. The reference temperature T_0 was also present in these new equations. As a result, we obtained equations using 23 parameters with temperature-like scaling factors to simulate the sequential firing patterns shown in Fig. 3.

The cell membrane of this model contains sodium, calcium, and potassium channels carrying a fast sodium current, I_{Na}, fast calcium current, I_{Ca}, and a potassium current, I_K, respectively. The sodium channel contains a fast-activated *m* gate and a fast-inactivated *h* gate upon depolarization. The calcium channel contains a fast-activated *d* gate and a slow-inactivated *f* gate. The potassium channel is controlled by an activated n gate. This membrane also contains a leak current, I_L. And then the membrane potential, V, is given by

$$\begin{aligned} -C_m\frac{dV}{dt} &= I_{Na}+I_{Ca}+I_K+I_L \\ &= \rho(T)\bar{g}_{Na}\frac{1}{1+e^{\left(\frac{V_m-V}{S_m}\right)}}h\{V-\sigma(T)V_{Na}\} \\ &\quad +\rho(T)\bar{g}_{Ca}\frac{1}{1+e^{\left(\frac{V_d-V}{S_d}\right)}}f\{V-\sigma(T)V_{ca}\} \\ &\quad +\rho(T)\bar{g}_K\, n\{V-\sigma(T)V_K\} \\ &\quad +\rho(T)\bar{g}_L\{V-\sigma(T)V_L\}, \end{aligned} \tag{1}$$

where C_m is the membrane capacitance. The temperature-dependent scaling factor, $\rho(T)$, is defined as $\rho(T)\equiv 1.3^{\frac{T-T_0}{10^{\circ}C}}$; the temperature coefficient of the single-channel conductance is Q_{10}=1.35 [18]. The other temperature-dependent scaling factor, $\sigma(T)$, is defined as $\sigma(T)\equiv\frac{T+273.15\,K}{T_0+273.15\,K}$. In Eq. (1), V_{Na}, V_{Ca}, V_K, and V_L are the Nernst potentials for the Na^+, Ca^{++}, K^+, and leak currents, respectively; $\bar{g}_{Na}$, $\bar{g}_{Ca}$, $\bar{g}_K$, and $\bar{g}_L$ are the maximal conductance for the respective currents. V_m and S_m, V_d and S_d are the half-maximal potentials and the slopes at these half-maximal potentials of the activation variables m and d, respectively. The inactivation variables h and f, and the activation variable n are all functions of voltage and time and these are described by the following differential equations,

$$\frac{dh}{dt}=\phi(T)\frac{(h_\infty-h)}{\tau_h}=\phi(T)\frac{\frac{1}{1+e^{\left(\frac{V_h-V}{S_h}\right)}}-h}{\frac{\bar{\tau}_h}{e^{\left(\frac{V_h-V}{2S_h}\right)}+e^{\left(\frac{V-V_h}{2S_h}\right)}}}, \tag{2}$$

$$\frac{df}{dt}=\phi(T)\frac{(f_\infty-f)}{\tau_f}=\phi(T)\frac{\frac{1}{1+e^{\left(\frac{V_f-V}{S_f}\right)}}-f}{\frac{\bar{\tau}_f}{e^{\left(\frac{V_f-V}{2S_f}\right)}+e^{\left(\frac{V-V_f}{2S_f}\right)}}}, \tag{3}$$

Table 2. Seven arrangements of temperature-dependent scaling parameters for maximum conductance and time constants

Models	Scaling parameters for maximum conductances				Scaling para. for the time constants	Scaling para. for Nernst potentials	Ref. temp. (°C)	Variables
	Na^+-current	K^+-current	Ca^+-current	Cl^--current				
Type 1	ρ (T)	ρ (T)	ρ (T)	1	Φ(T)	1	21	$\bar{g}_K$, and $\bar{\tau}_n$
Type 2	ρ (T)	ρ (T)	ρ (T)	1	Φ(T)	1	21	$\bar{g}_{Ca}$, and $\bar{\tau}_h$
Type 3	ρ (T)	ρ (T)	ρ (T)	1	Φ(T)	1	21	$\bar{g}_{Ca}$, and $\bar{\tau}_n$
Type 4	ρ (T)	ρ (T)	ρ (T)	1	Φ(T)	σ (T)	21	$\bar{g}_{Ca}$
Type 5	ρ (T)	ρ (T)	ρ (T)	ρ (T)	Φ(T)	1	23.2	$\bar{g}_{Ca}$, and $\bar{\tau}_h$
Type 6	ρ (T)	ρ (T)	ρ (T)	ρ (T)	Φ(T)	σ (T)	23.2	$\bar{g}_{Ca}$, and $\bar{\tau}_h$
Type 7	ρ (T)	ρ (T)	ρ (T)	1	Φ(T)	1	11	$\bar{g}_{Ca}$, and $\bar{\tau}_f$
Type 8	1	1	1	1	1	1		$\bar{g}_{Ca}$, and $\bar{\tau}_h$

Scaling para. for the time constants, scaling parameters for the time constants; Scaling para. for Nernst potentials, scaling parameters for Nernst potentials; Ref. temp., reference temperature.

$$\frac{dn}{dt}=\phi(T)\frac{(n_\infty-n)}{\tau_n}=\phi(T)\frac{\frac{1}{1+e^{\left(\frac{V_n-V}{S_n}\right)}}-n}{\frac{\bar{\tau}_n}{1+e^{\left(\frac{V-V_n}{2S_n}\right)}}}, \quad (4)$$

where the temperature-dependent scaling factor, $\phi(T)$, is defined as $\phi(T)\equiv 3^{\frac{T-T_0}{10^\circ C}}$; many enzyme reactions have a Q_{10} value near 3, as does the gating of many ion channels [18]. The sigmoidal steady-state inactivations, h_∞ and f_∞ are defined as $h_\infty\equiv 1/(1+\exp\left(\frac{V_h-V}{S_h}\right))$ and $f_\infty\equiv 1/(1+\exp\left(\frac{V_f-V}{S_f}\right))$, and the steady-state activation, n_∞, is defined as $n_\infty\equiv 1/(1+\exp\left(\frac{V_n-V}{S_n}\right))$. The parameters h_∞, f_∞, and n_∞ are functions of voltage and time. The relaxation time constants τ_h, τ_f, and τ_n are respectively defined as $\tau_h\equiv\bar{\tau}_h/(\exp(\frac{V_h-V}{2S_h})+\exp(\frac{V-V_h}{2S_h}))$, $\tau_f\equiv\bar{\tau}_f/(\exp(\frac{V_f-V}{2S_f})+\exp(\frac{V-V_f}{2S_f}))$, and $\tau_n\equiv\bar{\tau}_n/(1+\exp(\frac{V-V_n}{2S_n}))$, where $\bar{\tau}_h$, $\bar{\tau}_f$, and $\bar{\tau}_n$ are maximal time constants; these are also functions of voltage and time. The actual forms of these variables are described in equations (2)~(4). The variables V_h and S_h, V_f and S_f, V_n and S_n are the half-maximal potentials and the slopes at these half-maximal potentials of h, f, and n, respectively.

We modified the equations derived by Chay and Lee [6,7] for excitable cells by adopting temperature-like scaling factors defined in the Huber-Braun model. This modified Chay-Lee model is required to explain the temperature dependence of the sequence of the seven different firing patterns. Various combinations of $\rho(T)$, $\phi(T)$, and $\sigma(T)$ are shown in Table 2. Scaling factors in the type 1, 2 and 3 models have similar temperature-dependent scaling factors as those in the above mentioned paper by Braun et al. We tried to apply scaling factors that depend on temperature in this new equations as much as possible. To do this, we considered all eight combinations of scaling factors. Table 2 and 3 contains details of the eight different type models obtained by changing the temperature-dependent scaling factors. In type 1 model $\bar{g}_K$ and $\bar{\tau}_n$ were used as variables, and the temperature-dependent scaling factors used in the Huber-Braun cold receptor model were chosen. Although the reference temperature was 25°C in the Huber-Braun

Table 3. Numerical values of the parameters in the models. The first seven parameters are the same in all eight model types. For the middle 11 parameters, numerical values in bold type indicate the parameters that have different values from that used in type 1. The last five parameters denote variables

Para. in the model	Unit	Numerical values of the parameters in the models							
		Type 1	Type 2	Type 3	Type 4	Type 5	Type 6	Type 7	Type 8
C_m	$\mu F\ cm^{-2}$	1	1	1	1	1	1	1	1
$\bar{g}_L$	$\mu S\ cm^{-2}$	18	18	18	18	18	18	18	18
V_{Na}	mV	80	80	80	80	80	80	80	80
V_{Ca}	mV	140	140	140	140	140	140	140	140
V_L	mV	−71	−71	−71	−71	−71	−71	−71	−71
V_f	mV	−54	−54	−54	−54	−54	−54	−54	−54
S_m	mV	6.4	6.4	6.4	6.4	6.4	6.4	6.4	6.4
$\bar{g}_{Na}$	$\mu S\ cm^{-2}$	1,000	1,000	1,000	1,000	1,000	1,000	**1,300**	1,000
V_K	mV	−90	**−80**	**−80**	**−80**	**−80**	**−80**	**−80**	**−80**
V_m	mV	−12	−12	−12	−12	−12	−12	**−10**	−12
V_h	mV	−35	**−39**	**−39**	**−39**	**−40**	**−39**	**−40**	**−39**
V_d	mV	−48.4	−48.4	−48.4	**−49.4**	**−49.5**	**−49.5**	**−47.6**	**−49.0**
V_n	mV	15	15	15	15	15	15	**14.5**	15
S_h	mV	−5.4	−5.4	−5.4	**−5.5**	**−5.1**	**−5.5**	**−5.1**	**−5.5**
S_d	mV	5.7	5.7	5.7	**5.88**	**5.5**	5.7	**5.27**	**6**
S_f	mV	−8.5	−8.5	−8.5	−8.5	**−10**	**−10**	**−10**	**−10**
S_n	mV	15	15	15	15	15	15	**16**	15
T_0	°C	21	21	21	21	**23.2**	**23.2**	**11**	
$\bar{g}_{Ca}$	$\mu S\ cm^{-2}$	28	**Variable (13~32)**	**Variable (15~120)**	**Variable (9~20)**	**Variable (13~27)**	**Variable (7~27)**	**Variable (13.2~21)**	**Variable (9~27)**
$\bar{g}_K$	$\mu S\ cm^{-2}$	Variable (120~1,100)	**330**	**330**	**330**	**330**	**330**	**330**	**330**
$\bar{\tau}_h$	ms	160	**Variable (59~270)**	**200**	**120**	**Variable (123~440)**	**Variable (155~230)**	**1200**	**Variable (40~186)**
$\bar{\tau}_n$	ms	Variable (40~150)	**80**	Variable (65~700)	**80**	**80**	**80**	**80**	**80**
$\bar{\tau}_f$	s	100	**40**	100	**110**	**90**	**200**	**Variable (12.3~90)**	**60**

Para. in the model, parameters in the model.

model, in this model we took a value of 21°C as the reference temperature because this represents the middle of the temperature range (from 11°C to 31°C) of Experiment A. The type 2 and 3 models used the same combination of factors as type 1 model except that the variable $\bar{g}_{Ca}$, $\bar{\tau}_h$ was used in the type 2 and $\bar{g}_{Ca}$ in the type 3 instead of $\bar{g}_K$, $\bar{\tau}_n$ in type 1. The type 4 model is different from the type 1 because a scaling factor, σ(T) is considered in addition to the type 1 parameters. $\bar{g}_{Ca}$ is the only variable used in the type 4 model. The type 5 model differs from the type 1 model because a scaling factor for the maximum conductance of leak current is considered, and a new reference temperature, 23.2°C, is used. The type 6 model is the same as the type 5 except for an additional scaling factor, σ(T). The type 7 model is the same as the type 1 model except that the reference temperature is taken to be 11°C and the variables $\bar{g}_{Ca}$ and $\bar{\tau}_f$ are used instead of $\bar{g}_K$ and $\bar{\tau}_n$. Twenty one fixed parameters are used in the type 8 model and $\bar{g}_{Ca}$ and $\bar{\tau}_h$ are variables [19].

From these eight types of model, it was necessary to select the best type of model to properly explain the temperature dependence of the sequence of firing patterns. Each value of the first seven parameters in Table 3 was the same for all models. In the middle section of the table, numerical values in bold type indicate the parameter values that differ from the corresponding values in the type 1 model. The five parameters at the bottom of Table 3 are variables: $\bar{g}_{Ca}$, $\bar{g}_K$, $\bar{\tau}_h$, $\bar{\tau}_n$, and $\bar{\tau}_f$. $\bar{g}_{Ca}$ is a variable in all of these seven types of model except the type 1 model.

It is, however, necessary to check other merit points of the type 1 model. The first merit point is that the type 1 model was obtained using the same kind of temperature-dependent scaling factors used by the Huber-Braun cold receptor model. The second one is that the temperature range of the doublet in the experiment (between 24.5°C and 26.3°C) was similar to that in simulation results (between 24.0°C and 26.5°C). The last point to consider is that $\bar{g}_K$ and $\bar{\tau}_n$ were used as variables. These two variables are associated with the potassium channels. Interestingly, we found that the spiking pattern changed from beating to doublet (from Fig. 8E1 to E2), when potassium channel blockers, TEA and 4-AP were used. It is noteworthy that this change phenocopies the temperature-induced change from beating to doublets (from Fig. 4E3A to 4E4A). Therefore, the type 1 model was considered to be a suitable simulation model as it contains the potassium channel associated variables, $\bar{g}_K$ and $\bar{\tau}_n$. The procedure to draw figures using parameters of the type 1 model is as follows.

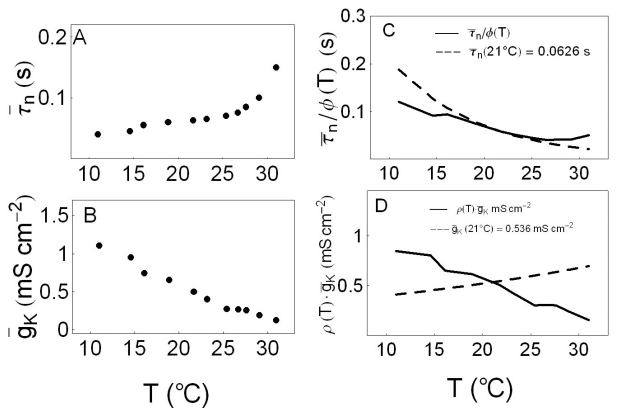

Fig. 6. Simulation variables. Panel A display the variation in $\bar{\tau}_n$ with respect to temperature. Panel B displays the variation in $\bar{g}_K$ with respect to temperature. Panel C displays $\bar{\tau}_n/\phi$(T). In this panel the dotted line displays the value of $\bar{\tau}_n/\phi$(T) when $\bar{\tau}_n$ is a constant value at reference temperature 21°C. The solid line in panel C displays $\bar{\tau}_n/\phi$(T) with $\bar{\tau}_n$ as a variable represented in panel A at the corresponding temperatures. At low (high) temperatures the value of $\bar{\tau}_n/\phi$(T) is smaller (larger) than the expected value, which is shown as a dotted line. Panel D displays ρ(T) · $\bar{g}_K$. In this panel the dotted line displays the value of ρ(T) · $\bar{g}_K$ when $\bar{g}_K$ is a constant value at reference temperature of 21°C. The solid line in this panel displays the value of ρ(T) · $\bar{g}_K$ with $\bar{g}_K$ a variable represented in panel B at the corresponding temperatures. Although the dotted line increase as temperature increase, the solid line decrease.

Computer simulation

The time traces of APs in Fig. 4S1 are plotted from the equations (1) to (4) at temperatures indicated in Fig. 4E1A using the values of the maximal potassium conductance and maximal potassium time constant in Fig. 4S1. Panels from Fig. 4S2 to Fig. 5S4 are also composed of the graphs plotted from these equations at temperatures indicated in the corresponding panels (from Fig. 4E2A to Fig. 5E4A) us-

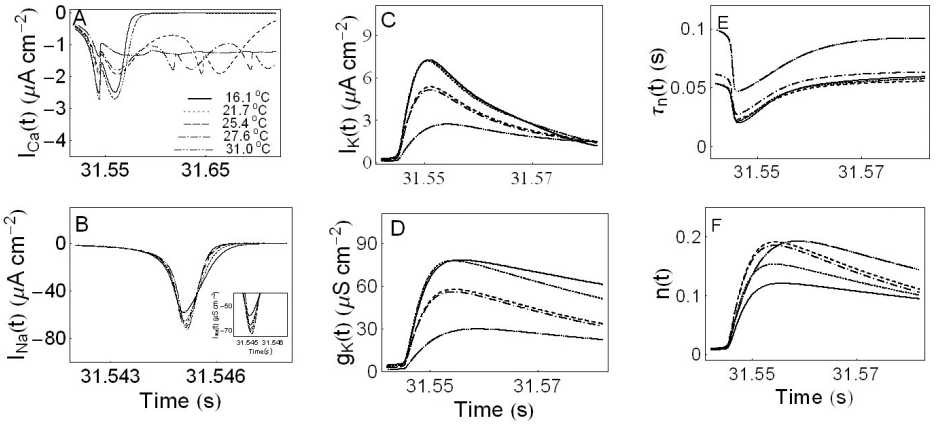

Fig. 7. Ionic currents and parameters as a function of time. Panel A, B, and C display I_{Ca}(t), I_{Na}(t), and I_K(t), respectively. The solid, dotted, dashed, dash-dotted, dashed-double-dotted lines in panels from A to F are used to represent the variables as a function of time at temperatures 16.1°C, 21.7°C, 25.4°C, 27.6°C, and 31°C, respectively. Panel D displays g_k(t). The potassium channel relaxation time constants τ_n(t) and the probabilities of openings for activation of the potassium channels n(t) as a function of time are shown in panels E and F, respectively.

ing the values of the corresponding potassium maximal conductances and maximal time constants shown in the panels from Fig. 4S2 to Fig. 5S4. In order to draw these graphs, we used the following numerical values in the type 1 model:

(1) membrane capacitance: $C_m=1\ \mu F cm^{-2}$;
(2) the Nernst potentials for ions: $V_{Na}=80$ mV, $V_{Ca}=140$ mV, $V_K=-90$ mV, $V_L=-71$ mV;
(3) the maximal conductance: $\bar{g}_{Na}=1{,}000\ \mu S\ cm^{-2}$, $\bar{g}_{Ca}=28\ \mu S\ cm^{-2}$, $\bar{g}_K$=variable ($120\sim1{,}100\ \mu S\ cm^{-2}$), $g_L=18\ \mu S\ cm^{-2}$;
(4) maximal time constants: $\bar{\tau}_h=0.16$ s, $\bar{\tau}_f=100$ s, $\bar{\tau}_n$ = variable ($0.040\sim0.150$ s);
(5) the half-maximal potentials: $V_m=-12$ mV, $V_h=-35$ mV, $V_d=-48.4$ mV, $V_f=-54$ mV, $V_n=15$ mV;
(6) the slopes at the half-maximal potentials: $S_m=6.4$ mV, $S_h=-5.4$ mV, $S_d=5.7$ mV, $S_f=-8.5$ mV, $S_n=15$ mV;
(7) reference temperature: $T_0=21^oC$.

The values of the variables $\bar{g}_K$ and $\bar{\tau}_n$ used in each simulation are shown in the bottom panels of Fig. 4 and 5.

To compare the simulation results with experimental results, eight sets of three figures are drawn in Fig. 4 and 5. The time traces of membrane potentials displayed in the top panels of Fig. 4 and 5 (from Fig. 4E1A to Fig. 5E4A) show a part of data from Experiment A shown in Fig. 3, whereas those in the middle panels (from Fig. 4E1B to Fig. 5E4B) show a part of data from Experiment B. These sets of figures are arranged from low to high temperatures. Simulation results of the type 1 model are displayed in the bottom panels in Fig. 4 and 5 (from Fig. 4S1 to Fig. 5S4); these figures were obtained by solving equations in modified Chay-Lee model using Mathematica 5.1. To summarize, the bottom panels of Fig. 4 and 5 show the simulation results of this model at the temperatures shown in top panels; the used values of variables are shown in bottom panels.

In Fig. 4 panels E1A, E1B, and S1 show silent patterns. Panels E2A , E3A, E2B, E3B, S2, and S3 show beating, whereas panels E4A, E4B, and S4 show doublet patterns. In Fig. 5, panels E1A, E1B and S1 show beating-chaos, whereas panels E2A, E2B, and S2 show bursting-chaos. Panels E3A, E3B, and S3 show square-wave bursting, whereas panels E4A, E4B, and S4 show bursting-oscillations. Although the AP amplitudes in the simulation results (panels from Fig. 4S1 to Fig. 5S4) and the corresponding experimental results (from Fig. 4E1A to Fig. 5E4A) are slightly different, the frequencies of the time series of simulated APs are all very similar to the corresponding experimental results. This is in line with the fact that specific intensity information of environmental stimulus is transformed into a corresponding AP frequency in sensory receptors. Therefore, the simulation results of these eight model types can be interpreted as similar results to the experimental ones despite a little discrepancy in the AP amplitude simulation.

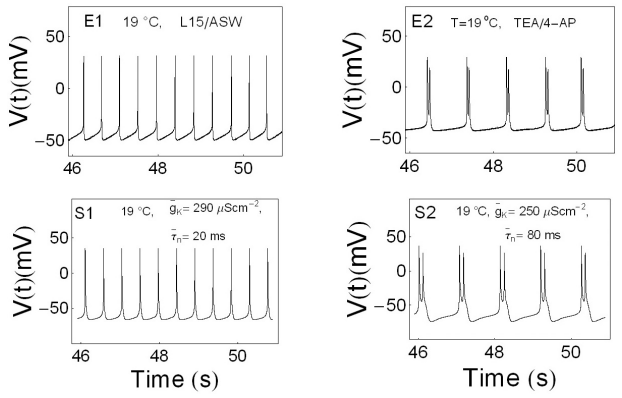

Fig. 8. Comparison of beating and bursting signals influenced or uninfluenced by drugs with simulation results. Panel E1 and E2 represents time series of APs without drug and with the treatment of drugs mixed with 10 mM TEA and 10 mM 4-AP, respectively. Panel S1 and S2 represents the results of computer simulation with modified Chay-Lee model with temperature-like scaling factors.

Fig. 6A and Fig. 6B displays the values of variables, $\bar{\tau}_n$ and $\bar{g}_K$, respectively, with respect to temperature. Fig. 6C displays the maximum time constant $\bar{\tau}_n$, divided by the temperature-like scaling factor $\phi(T)$, $\bar{\tau}_n/\phi(T)$ as a function of temperature. The solid line in this figure displays $\bar{\tau}_n/\phi(T)$ where $\bar{\tau}_n$ varies with temperature with each value in the panel A; at low temperatures, the values of $\bar{\tau}_n/\phi(T)$ are lower, and at high temperatures those are higher than the expected values, which is shown as a dotted line in this panel. Fig. 6D displays the maximum potassium conductance, $\bar{g}_K$, multiplied by the temperature-like scaling factor $\rho(T)$, i.e., $\rho(T)\cdot\bar{g}_K$. The solid line in this panel displays $\rho(T)\cdot\bar{g}_K$ where g_K varies with temperature with each value in the panel B; the values of $\rho(T)\cdot\bar{g}_K$ decrease, yet the expected values of these increase as the temperature increases.

Fig. 7A, B, C displays the calcium current, $I_{Ca}(t)$, the sodium current, $I_{Na}(t)$, and the potassium current, $I_K(t)$, as functions of time, respectively. The solid, dotted, dashed, dash-dotted, dashed-double dotted lines in panels from A to F are used to represent the variables as a function of time at temperatures 16.1°C, 21.7°C, 25.4°C, 27.6°C, and 31°C, respectively. As shown in Fig. 7A the maximum calcium currents increase as the temperature rises until 21.7°C and then decrease, but sodium currents increase as the temperature increases as shown in Fig. 7B and inset figure. The maximum potassium current decreases as the temperature increases. This is shown in Fig. 7C. Time series of the potassium conductance, $g_K(t)$ are shown in Fig. 7D. The maximum potassium conductance also decreases as the temperature increases. Time series of the potassium time constants $\tau_n(t)$ are shown in Fig. 7E. The maximum values of $\tau_n(t)$ decrease as the temperature rises until 25.4°C and then decrease as the temperature increases further. Fig. 7F displays a time series of the probability of the opening of the potassium channel activation gate, n(t). In this panel, the maximum values of n(t) at high temperatures are larger than those at low temperatures. However, we need more experimental data to investigate the exact mechanisms inherent in determining the temperature-dependent properties of *Aplysia* neurons. We then carried out the experiments with potassium channel blockers since potassium channels are known to critically regulate the shape of AP and the firing pattern.

We used two distinct, specific potassium channel blockers TEA and 4-AP to find inter-relationships between TEA, 4-AP and APs. Our electrophysiological recording data revealed that TEA and 4-AP produced distinct pattern changes. Treatment of 10 mM TEA made AP frequency rise, width of APs wider, negative peak value rise, and amplitude of APs decrease. Treatment of 10 mM 4-AP made mostly opposite effects. It made AP frequency fall and width of APs narrower, and amplitude of APs increase, but

negative peak value is not much affected. Mixing both 10 mM TEA and 10 mM 4-AP showed similar results to 10 mM TEA treatment (*data not shown*). We also found that the spiking pattern changed from beating (Fig. 8E1) to doublet (Fig. 8E2) at 19°C when mixed K^+ channel blockers (10 mM TEA and 10 mM 4-AP) were bath applied to *Aplysia* neuron. It is noteworthy that this is similar to the change from beating (Fig. 4E3A)to doublets (Fig. 4E4A) when temperature was changed from 21.7°C to 25.4°C. Fig. 8S1 and S2 represents the results of computer simulation with modified Chay-Lee model using the values of variables shown in each panel at 19°C.

Ionic currents and parameters analyzed in the experiments with drugs (Fig. 8E1, E2, S1, and S2) or changing temperatures (Fig. 4E3A, E4A, S3, and S4) are shown in Fig. 9 as a function of time. Fig. 9A and B display $I_K(t)$ and $g_K(t)$, respectively. The solid, dotted lines in the panels from A to D shows the time series of ionic currents and parameters without drugs and with drugs (10 mM TEA and 10 mM 4-AP) at 19°C, respectively. The dashed and dash-dotted lines in the panels from A to D show the time series of those parameters in the firing state of beating at 21.7°C and in the spiking state of doublet at 25.4°C, respectively. The time series of the potassium channel relaxation time constant, $\tau_n(t)$ and the probabilities of the openings for the activation of the potassium channels, n(t) are shown in the panels C and D. The maximum value of $\tau_n(t)$ increases whereas the maximum value of n(t) decreases as temperature increases.

DISCUSSION

Modified Chay-Lee model with temperature-dependent scaling factors

By analyzing the equations in modified Chay-Lee model, we attempted to trace the mechanism underlying change of the various spike patterns as a response to a periodic change in temperature in *Aplysia* neurons.

It is known that the solutions of the dynamic equations developed by Chay and Lee [6,7] simulate six consecutive spiking patterns with the increasing function of maximal relaxation time constant $\bar{\tau}_h$ (or $\bar{\tau}_n$). Although these equations does not contain any temperature-dependent scaling factors, the Huber-Braun cold receptor model [14,15] contains temperature-like scaling factors; the maximal conductances of currents were multiplied by the temperature-dependent scaling factor $\rho(T)$, and the maximal time constants were divided by the temperature-dependent scaling factor $\phi(T)$. To reproduce by simulation the seven different types of signals during an increase (or decrease) in temperature, a set of equations that contain temperature-dependent scaling factors are required; the aim was to find neuronal equations capable of simulating at once all the various spiking patterns shown in Table 1. As a result, we crafted a set of equations by modifying the Chay-Lee model to include temperature-dependent scaling factors for the ionic currents and for the ionic kinetics used in the Huber-Braun cold receptor model; computer simulation using the parameter values in the type 1 model was reasonably good. However, the simulated AP amplitudes displayed in Fig. 4S1～Fig. 5S4 were slightly larger than the experimental results displayed in Fig. 4E1A～Fig. 5E4A. Nevertheless, the frequencies of simulation and experimental results were similar when compared at the corresponding temperatures. This demonstrates that we can trace the ionic mechanism of the firing pattern change in response to temperature change in *Aplysia* neurons by solving these equations of modified Chay-Lee model and analyzing the simulation results.

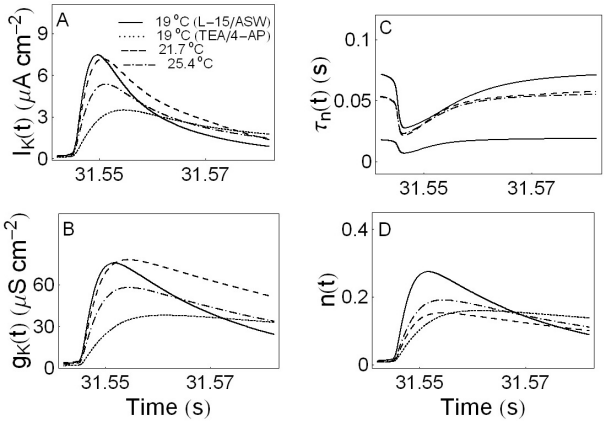

Fig. 9. Ionic currents and parameters as a function of time. Panel A and B display $I_K(t)$ and $g_K(t)$, respectively. The potassium channel relaxation time constants $\tau_n(t)$ and the probabilities of openings for activation of the potassium channels n(t) as a function of time are shown in panels C and D, respectively. The solid, dotted, dashed, and dash-dotted lines in panels from A to D indicate L15/ASW medium control without drugs at 19°C, L15/ASW medium containing 10 mM TEA and 10 mM 4-AP at 19°C, L15/ASW medium at 21.7°C, and L15/ASW medium at 25.4°C, respectively.

Ionic mechanism of temperature-driven firing pattern change

The modified Chay-Lee model contains a fast I_{Na} and slow I_{Ca}. The characteristics of these inward currents are similar to each other because the d gate in I_{Ca} opens as fast as the m gate in I_{Na}. $\bar{\tau}_f$ controls the burst periodicity, whereas $\bar{\tau}_h$ and $\bar{\tau}_n$ are related to the amplitude and frequencies of spikes [6]. As shown in Table 3, $\bar{\tau}_h$, $\bar{\tau}_f$, or $\bar{\tau}_n$ are variables in the simulation. These parameters with temperature-dependent scaling factors decrease as temperature increases. This means that the h, f, and n gates open faster at high temperature than at low temperature. The maximum conductances $\bar{g}_{Ca}$, $\bar{g}_{Na}$, and $\bar{g}_K$ with the temperature-dependent scaling factors theoretically increase as temperature increases, whereas $\bar{g}_K$ decreases as temperature increases as shown in Fig. 6B. The calcium currents, $I_{Ca}(t)$ have maximum value at 21.7°C and decrease at high temperatures as shown in Fig. 7A. In Fig. 7B and C, however, maximum values of $I_{Na}(t)$ and $I_K(t)$ increase and decrease as temperature increases, respectively. As shown in Table 3, we used five variable parameters in the simulation: $\bar{g}_{Ca}$, $\bar{g}_K$, $\bar{\tau}_h$, $\bar{\tau}_n$, and $\bar{\tau}_f$. Among the five variables, only two are used in the type 1 model: $\bar{g}_K$ and $\bar{\tau}_n$; $\bar{\tau}_n$ is one of the three variables of maximal time constants, and $\bar{g}_K$ is one of the two variable of maximal conductances. From these figures, it may be supposed that the temperature dependence of sodium and calcium currents is driven by the temperature-dependent potassium current. Thus, the voltage-dependent potassium current is assumed to play a leading role in the temperature-sensitive reactions of neurons

in *Aplysia* abdominal ganglion. However, more experiments have to be performed for further analysis with other channel blockers or other currents [20].

How can we trace the mechanism of change between the various spike patterns in *Aplysia* neurons in response to a periodic change in temperature by analyzing the modified Chay-Lee model? To address the issue, we can present the following procedure. First, it is necessary to set up nonlinear differential equations with temperature-like scaling factors and experiment results are to be simulated with these equations. Second, other experiments should be performed with ion channel blockers and these experimental results have to be simulated with revised equations. During the repeated procedure, if all of the AP parameters [17] are simulated well, then the problems will be resolved. Let's give an instance. In a set of experiments, we found that the spiking pattern change from beating to doublet (from Fig. 8E1 to E2) at room temperatures in the presence of K^+ channel blockers was similar with the changes from beating to doublets caused by change in temperature only (from Fig. 4E3A to E4A). Therefore, some of the mechanisms inherent in the temperature dependencies of *Aplysia* neurons can be expressed by analyzing the results of the experiments using modified Chay-Lee model.

TEA or 4-AP reduced potassium current at a concentration of 10 mM and blocked ion conduction through potassium channels in a voltage-dependent manner [21]. However, n(t) decreased and $\bar{\tau}_n$ increased when TEA was applied [22]. These results were consistent with the simulation results obtained using modified Chay-Lee model and potassium current and conductance decreased, but $\bar{\tau}_n$ increased as drugs (TEA/4-AP) were applied (Fig. 8S1, Fig. 8S2). It would be interesting to perform more experiments in the future using more channel blockers or at different temperatures with different firing patterns to examine how reliably our modified Chay-Lee model can simulate experimental results.

Concluding remarks

When the temperature was increased from 11°C to 31°C, the firing patterns changed sequentially from silent to continuous spiking, doublets, beating-chaos, bursting- chaos, square-wave bursting, and bursting-oscillation sequentially. We wanted to develop a set of equations to describe these firing pattern changes and tried to apply temperature-dependent scaling factors in modified Chay-Lee model; as a result, 23 temperature dependent parameters were used in these equations. Figures were drawn by solving these equations in this model using Mathematica 5.1. Although the simulated AP amplitudes were slightly bigger than those in the experimental results, the frequencies of the simulated and experimental results were very similar to each other. These results clearly suggest that our model equations could trace the ionic mechanism underlying the firing pattern changes in response to temperature change in *Aplysia* neurons by analyzing the solutions of modified Chay-Lee model. As a result, the voltage-dependent potassium current seems to play a leading role in the temperature dependence of neurons in *Aplysia* abdominal ganglion. Therefore, it will be of great interest to apply our new model equations to simulate the temperature dependence of the 14 AP parameters that we identified in *Aplysia* neurons in the previous study [17].

ACKNOWLEDGEMENTS

This work was supported by a research grant from Jeju National University in 2007 and supported in part by URP program in KAIST. NGH is most grateful to Prof. Jang-Ho Cha for his helpful advice and suggestions throughout the course of this work and for his generosity in allowing experiments to be conducted at MGH. BKK was supported by the National Creative Research Initiative Program and the WCU program. KL was supported by the Basic Science Research Program of the Ministry of Education, Science and Technology (2011-0028240).

REFERENCES

1. **Carpenter DO.** Temperature effects on pacemaker generation, membrane potential, and critical firing threshold in *Aplysia* neurons. *J Gen Physiol.* 1967;50:1469-1484.
2. **Moffett S, Wachtel H.** Correlations between temperature effects on behavior in *Aplysia* and firing patterns of identified neurons. *Mar Behav Physiol.* 1976;4:61-74.
3. **Carpenter DO, Alving BO.** A contribution of an electrogenic Na^+ pump to membrane potential in *Aplysia* neurons. *J Gen Physiol.* 1968;52:1-21.
4. **Fletcher SD, Ram JL.** High temperature induces reversible silence in *Aplysia* R15 bursting pacemaker neuron. *Comp Biochem Physiol.* 1991;98A:399-405.
5. **Hakozaki S, Matsumoto M, Sasaki K.** Temperature-sensitive activation of G-protein regulating the resting membrane conductance of *Aplysia* neurons. *Jpn J Physiol.* 1989;39:115-130.
6. **Chay TR.** Bursting excitable cell models by a slow Ca^{2+} current. *J Theor Biol.* 1990;142:305-315.
7. **Chay TR, Lee YS.** Bursting, beating, and chaos by two functionally distinct inward current inactivations in excitable cells. *Ann N Y Acad Sci.* 1990;591:328-350.
8. **Hensel H, Huopaniemi T.** Static and dynamic properties of warm fibres in the infraorbital nerve. *Pflugers Arch.* 1969;309: 1-10.
9. **Hensel H, Schäfer K.** Static an dynamic activity of cold receptors in cats after long-term exposure to various temperatures. *Pflugers Arch.* 1982;392:291-294.
10. **Schäfer K, Braun HA, Kürten L.** Analysis of cold and warm receptor activity in vampire bats and mice. *Pflugers Arch.* 1988;412:188-194.
11. **Hensel H.** Static and dynamic activity of warm receptors in Boa constrictor. *Pflugers Arch.* 1975;353:191-199.
12. **Kim YD, Cho MH, Kwon SC.** Myoplasmic [Ca^{2+}], crossbridge phosphorylation and latch in rabbit bladder smooth muscle. *Korean J Physiol Pharmacol.* 2011;15:171-177.
13. **Kim KS, Shin DH, Nam JH, Park KS, Zhang YH, Kim WK, Kim SJ.** Functional expression of TRPV4 cation channels in human mast cell line (HMC-1). *Korean J Physiol Pharmacol.* 2010;14:419-425.
14. **Braun HA, Huber MT, Dewald M, Schäfer K, Voigt K.** Computer simulations of neuronal signal transduction: the role of nonlinear dynamics and noise. *Int J Bifurcation Chaos.* 1998;8: 881-889.
15. **Finke C, Freund JA, Rosa E Jr, Braun HA, Feudel U.** On the role of subthreshold currents in the Huber-Braun cold receptor model. *Chaos.* 2010;20:045107.
16. **Lim CS, Chung DY, Kaang BK.** Partial anatomical and physiological characterization and dissociated cell culture of the nervous system of the marine mollusc *Aplysia kurodai. Mol Cells.* 1997;7:399-407.
17. **Hyun NG, Hyun KH, Lee K, Kaang BK.** Temperature Dependence of Action Potential Parameters in *Aplysia* Neurons. *Neurosignals.* 2011 (in press).
18. **Hille B.** Ion channels of excitable membranes. 3rd ed. Sun-

derland Mass: Sinauer; 2001. 366 p.
19. **Hyun NG.** The brain and the mind. 1st ed. Jeju: Jeju Nat Univ; 2007. 321-338 p.
20. **Wang LY, Fedchyshyn MJ, Yang YM.** Action potential evoked transmitter release in central synapses: insights from the developing calyx of Held. *Mol Brain*. 2009;2:36.
21. **Volk KA, Matsuda JJ, Shibata EF.** A voltage-dependent potassium current in rabbit coronary artery smooth muscle cells. *J Physiol*. 1991;439:751-768.
22. **Spruce AE, Standen NB, Stanfield PR.** The action of external tetraethylammonium ions on unitary delayed rectifier potassium channels of frog skeletal muscle. *J Physiol*. 1987;393: 467-478.